eXPRESS Polymer Letters Vol.13, No.2 (2019) 199–212
Available online at www.expresspolymlett.com
https://doi.org/10.3144/expresspolymlett.2019.16

Crystallization and dielectric behavior of PLA and PHBV in PLA/PHBV blends and PLA/PHBV/TiO_2 nanocomposites

*S. Gasmi, M. K. Hassan, A. S. Luyt**

Center for Advanced Materials, Qatar University, PO Box 2713, Doha, Qatar

Received 31 July 2018; accepted in revised form 20 September 2018

Abstract. The morphology, crystallization behavior and mechanical properties of PLA, PHBV and their blends and nanocomposites with TiO_2 as filler were investigated. An uncommon morphological change was observed with increasing PLA content in the blends, and this complicated the isothermal crystallization kinetics analyses of the different samples. It was, for example, observed that PLA, which do not normally crystallize during the cooling of the sample, showed isothermal crystallization for certain blend compositions. TiO_2 was found to be mainly present in the PLA phase, which was also confirmed through broadband dielectric analysis. The blend composition, as well as the presence of TiO_2 nanoparticles, had an influence on the cold crystallization of the PLA. The tensile properties changed with blend and nanocomposite composition, and these changes could to a certain extent be related to the respective morphologies. Very little could be said about differences between the melting behavior of the different samples, because the PLA and PHBV melted at almost exactly the same temperature.

Keywords: *biodegradable polymers, morphology, crystallization behavior, dielectric properties, mechanical properties*

1. Introduction

Poly(lactic acid) (PLA) and poly(hydroxybutyrate-*co*-valerate) (PHBV) are both biodegradable polymers with properties comparable to commercial, petrochemical-based polymers. PLA is derived from renewable plant resources like corn and sugar beets. Although it has fairly good properties, it has a low heat deflection temperature, weak resistance to environmental conditions of high temperature and humidity, low flexibility, a long mold cycle time and low durability, which make it unsuitable for more sophisticated applications. PHBV is also biodegradable and biocompatible, and can be obtained from renewable resources. However, PHBV is associated with several weaknesses, such as having a low thermal stability, being expensive, showing brittle behavior and weak mechanical properties, and is difficult to process [1]. Blending these two polymers may provide a material with the best properties from each polymer. However, the presence of the one polymer in a blend may influence the crystallization behavior of the other polymer, and as a result change its crystallinity-related properties.

Very little work has previously been published on the crystallization behavior of these blends and nanocomposites. Some work has been done on unblended PLA and its nanocomposites. It was found that the presence of TiO_2 nanoparticles nucleated PLA crystallization and cold crystallization, but decreased its spherulitic growth rate [2]. PLA and its nanocomposite with clay were found to follow Avrami isothermal crystallization behavior from the melt and also from the amorphous solid state [3]. The Avrami exponents in all cases were found to be two, and it was found that the presence of nano clay increased the crystallization rate. The maximum crystallization rates were in the 105–125 °C temperature region. Similar crystallization was observed for PLA and

*Corresponding author, e-mail: aluyt@qu.edu.qa

PLA/talc composites [4]. However, in this case the authors found different values of the Avrami exponent for PLA and PLA/talc, indicating that PLA in the presence of talc showed two-dimensional growth on a lamellar structure. PHBV normally has a very low degree of heterogeneous nucleation because of its purity. Addition of cellulose nanocrystals effectively nucleated PHBV and increased its crystallization rate, but decreased its spherulite size [5].

There were several studies on PLA/PHBV blends, but only two reports could be found where the crystallization of these blends was investigated [6, 7]. These blends were found to exhibit Newtonian flow behavior, but PLA/PHBV/clay nanocomposites exhibited shear-thinning behavior [8]. The nanoclay restricted the relaxation of the polymer chains and significantly improved the crystallinity of PHBV in the blend, leading to higher modulus values and increased complex viscosity [9, 10]. Increasing amounts of PLA in the blends increased the modulus and complex viscosity values [11, 12]. The presence of natural fibres in PLA/PHBV blends increased the tensile stiffness and strength [13]. Increasing amounts of PLA in the blends increased the flexural strength and modulus, but the viscosity did not change from that of PHBV [14, 15]. The thermal stability, flammability resistance, stress at break and elongation at break of PHBV/PLA blends were found to increase with increasing PLA content [11], while the elastic modulus decreased. The presence of clay in these blends further enhanced the tensile properties, dynamic modulus and thermal stability of these blends [9, 10]. Mofokeng and Luyt [16] investigated the dynamic mechanical properties of PLA/PHBV blends and their nanocomposites with TiO_2. They found that the E' values between the glass transitions of PLA and PHBV depended on the blend compositions and morphologies, and that the presence of TiO_2 nanoparticles had little effect on the E' values of all the investigated blends.

A morphological investigation of the blends showed the crystallization of fine dispersed PHBV domains in the amorphous PLA matrix, resulting in rubbery particles. The ductility and toughness of the PLA was improved by the incorporation of 10–30% PHBV [17]. Dynamic mechanical analysis as function of frequency of the blends showed a decreasing activation energy with an increase in PLA content, indicating some molecular interaction between the two components [18]. PLA contained a large number of crystals, while PHBV presented a smaller number of crystalline nuclei, but larger crystals. Non-isothermal crystallization kinetics of PLA/PHBV blends showed that the dynamic crystallization of these blends can be well described by Mo's theoretical model [7]. A typical spherulitic morphology was observed, but the morphologies were complex for blends containing the two polymers in intermediate mass ratios. Hosoda *et al*. [6] observed a significantly decreased PHBV spherulite size after the incorporation of branched PLA, and remarkably higher crystallization rates after incorporation of both linear and branched PLA, which showed that the PLA was an effective heterogeneous nucleating agent. Electrospun PLA/PHBV blend fibres showed a decrease in the crystallinity of the PHBV fraction as its ratio in the blend increased, while the PLA crystallinity was found to be unaffected by the blend ratio, and the tensile strength of the blends was higher than that of PHBV [19]. Richards *et al*. [20] found the crystallinity of PHBV to be unaffected by the presence of PLA, but Zembouai *et al*. [12] found increasing PLA crystallinity due to the finely dispersed PHBV crystals acting as a nucleating agent for PLA.

A degradation analysis of PHBV and PHBV/TiO_2 composites showed that the presence of TiO_2 significantly increased the hydrolytic degradation of PHBV in a strong base medium, as well as its photocatalytic degradation [21]. Another study [22] found that the hydrolytic degradation of PLA was initially accelerated by the presence of TiO_2, but that the crystallinity increased with increasing degradation, which again slowed down the degradation process. It was also found that the degradation started at the interface between PLA and TiO_2, and that it was affected by the TiO_2 content and dispersion. As in the case of PHBV, the photodegradability of PLA was increased in the presence of TiO) nanoparticles, although the opposite was observed for TiO_2 nanowires [22]. Mofokeng and Luyt [23] reported the results of a thorough investigation into the thermal degradation behavior of PLA/PHBV blends and their nanocomposites with TiO_2.

It is known that the two polymers, but especially PLA, biodegrade fairly slowly, and addition of TiO_2 nanoparticles (that are optically active) may assist with the initiation of the UV-degradation of these polymers and their blends. The presence and location of TiO_2 in the PLA/PHBV blends should also have an influence on the crystallization behavior and kinetics

of the two polymers, as well as on their dielectric behavior. This project was aimed at investigating the influence of blending and the addition of TiO_2 nanoparticles on the cold crystallization behavior of PLA (its crystallization kinetics could not be investigated since the type of PLA we used was an amorphous polymer which crystallized only on heating), the crystallization behavior and kinetics of PHBV, and the relation of the dielectric permittivity of the different blends and nanocomposites to their respective morphologies.

2. Materials and methods

2.1. Materials

The poly(lactic acid) (PLA) used in this study is a high molar mass biopolymer (Ingeo™ Biopolymer 2003D), obtained from NatureWorks, LLC (USA). It is transparent with a density of 1.24 g·cm^{-3}, melt flow index of 6.0 g/10 min @ 2.16 kg/210 °C, glass transition and heat distortion temperatures of ~55 °C, melting temperature of ~150 °C, tensile strength of 60 MPa, tensile modulus of 3.6 GPa, elongation at break of 6%, and notched Izod impact strength of 0.16 J·cm^{-1}. The PHB88/PHV12 poly(hydroxybutyrate-*co*-valerate) (PHBV) was purchased from Goodfellow in the UK. It has a density of 1.25 g·cm^{-3}, tensile strength and modulus of respectively 23 and 500 MPa, and a melting point of 156 °C. It has a weak glass transition around 0 °C. The rutile titanium(IV)oxide (TiO_2) nanopowder with particle sizes <100 nm and 99.5% purity was obtained from Sigma-Aldrich.

2.2. Preparation method

The samples were prepared via melt-mixing using a Brabender Plastograph. The polymers were dried in a vacuum desiccator at 80 °C for four hours prior to mixing. The 25/75, 50/50, and 75/25 w/w PLA/PHBV blends and their nanocomposites with 3 phr TiO_2 were mixed at 170 °C and 30 rpm screw speed for ten minutes. The samples were compression moulded into 2 mm thick sheets at the same temperature for 5 minutes using a hydraulic press at a pressure of 50 bar.

2.3. Characterization methods

Scanning electron microscopy (SEM) analyses of the samples were performed using an FEI Quanta 200 electron microscope at an accelerating voltage of 2–5 kV. The samples were fractured in liquid nitrogen and sputter gold coated for 30 sec using an Agar sputter coater.

Transmission electron microscopy (TEM) images were obtained using a Philips CM100 TEM (at 60 kV). Sections were cut at –120 °C using a Leica UFC-6 cryo-microtome. 100–150 nm thin sections were collected on copper grids and viewed.

Dielectric measurements were performed using a Novocontrol GmbH Concept 40 broadband dielectric spectrometer (Montabaur, Germany), and data were collected over the frequency range 0.1 Hz–3 MHz at fixed temperatures in the range of –100 to 150 °C. Sample discs of 2 cm diameter were sandwiched between two gold-coated copper electrodes of 2 cm diameter and then transferred to the instrument for data collection.

The DSC analyses were performed in a Perkin Elmer DSC8500 differential scanning calorimeter. The samples (5–10 mg) were heated from 0 to 190 °C at 10 °C·min^{-1}, cooled to 0 °C at the same rate, and reheated to 190 °C at the same rate.

The isothermal crystallization kinetics analysis of neat PHBV and PHBV in the blends and nanocomposites was performed using an Origin™ software plug-in developed and described by Lorenzo *et al*. [24]. The crystallization exotherms were obtained by using a Perkin Elmer DSC8500 differential scanning calorimeter. The samples were heated to 190 °C at 60 °C·min^{-1}, held at this temperature for 3 min. to remove any trace of crystallinity, cooled to a pre-established crystallization temperature at 60 °C·min^{-1}, and held at this temperature for 15-20 min. while recording the isothermal crystallization exotherm. This procedure was repeated for a number of pre-established crystallization temperatures for each sample composition.

3. Results and discussion

3.1. Morphologies of blends and nanocomposites

The SEM micrograph in Figure 1a–1c show the morphologies of 25/75, 50/50 and 75/25 w/w PLA/PCL blends. Figure 1a clearly shows a sea-island morphology, with PLA spheres dispersed in the PHBV matrix. Although the micrograph does not show clear cavities around the spheres that would indicate weak interaction between the two polymers, there are no fractured spheres visible and one would assume that the interaction between the PLA chains is much stronger than the interaction between the PLA and

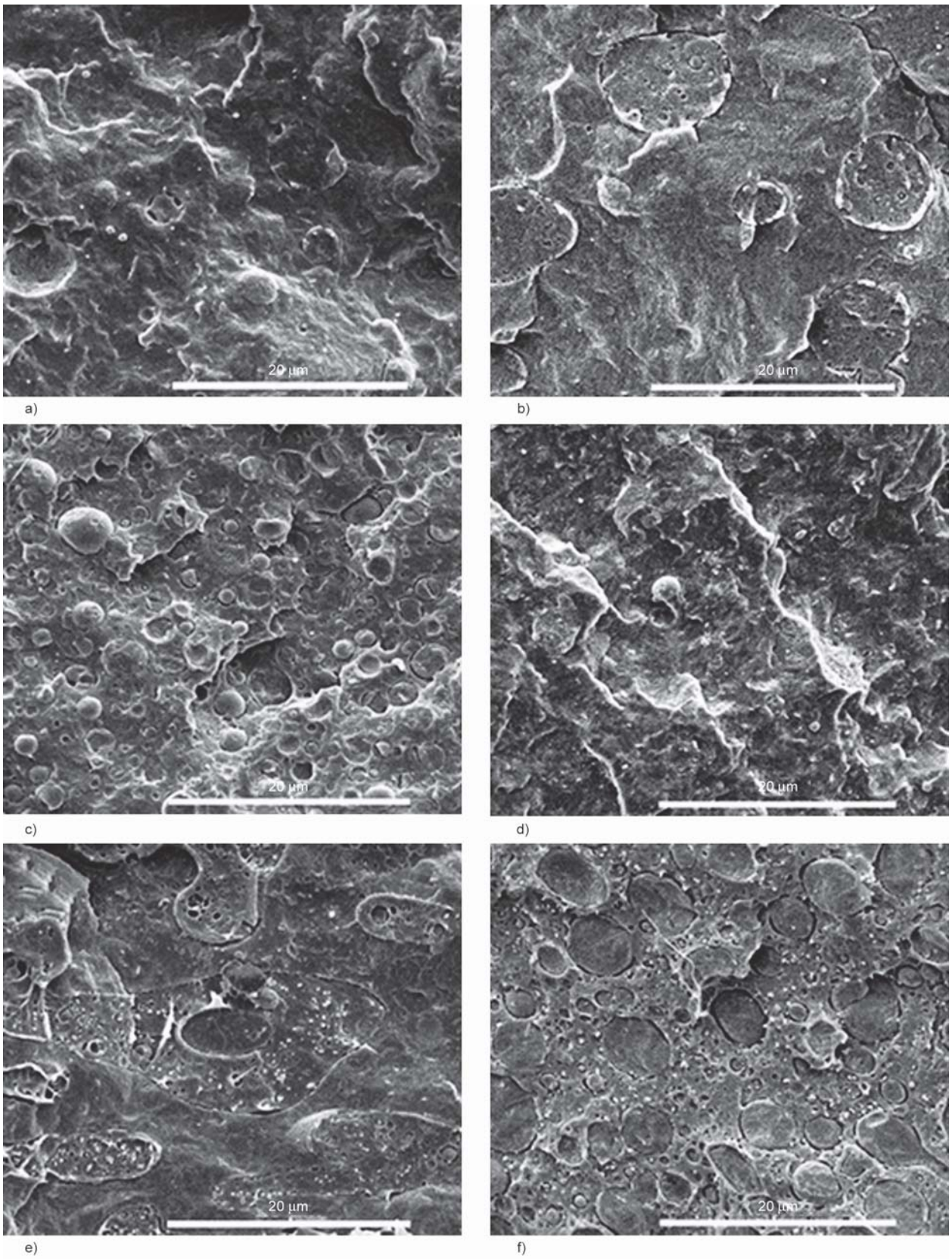

Figure 1. SEM micrographs of (a) 25/75, (b) 50/50, and (c) 75/25 w/w PLA/PHBV blends, and (d) 25/75 w/w PLA/PHBV + 3 phr TiO_2, (e) 50/50 w/w PLA/PHBV + 3 phr TiO_2 and (f) 75/25 w/w PLA/PHBV + 3 phr TiO_2.

the PHBV. Figure 1b does, however, show a very interesting phenomenon. Although one would expect a clear co-continuous morphology at this blend composition, it is clear from this micrograph that there

are still spheres of one polymer dispersed in a matrix of the other polymer. However, these spheres are much larger than the ones observed in Figure 1a, and there are clear cavities around these spheres. The most interesting observation, however, is the presence of very small spheres inside the bigger spheres. Figure 1c again shows the presence of unfractured spheres, probably PHBV, inside a continuous matrix, probably PLA.

An explanation for this phenomenon would be that PLA/PHBV blends do not follow the normal route of sea-island morphology through co-continuous morphology to sea-island morphology as one changes the composition from PLA being the minority phase to PHBV being the minority phase. The observations in Figure 1a–1c may be explained as follows: As the amount of PLA in the PLA/PHBV blend increases, the sizes of the PLA spheres increase, but at the same time the PHBV starts crystallizing as smaller spheres inside the bigger, amorphous PLA spheres. Further increases in the amounts of PLA in the blends cause increases in the sizes of the PLA spheres, and also increases in the sizes of the PHBV spheres embedded in the PLA spheres. This process continues until the PLA spheres merge to form the continuous matrix, which contains the PHBV spheres.

Figure 1d–1f and Figure 2 clearly shows that the TiO_2 nanoparticles have a stronger affinity for PLA than for PHBV, although a fair amount of these nanoparticles are visible in the PHBV phase. Close inspection of Figure 1d–1f shows the following:

(1) When PLA is the minority phase (Figure 1d), the PLA spheres are visible in the micrograph with the TiO_2 nanoparticles (visible as white spots in the micrograph) are clearly more concentrated on the surfaces of the spheres, although these white spots can also be observed in the continuous phase part of the micrograph.

(2) Figure 1e confirms the conclusions we have drawn from our observations in Figure 1b. This micrograph clearly shows larger spheres or ellipsoids that contain most of the nanoparticles, in a

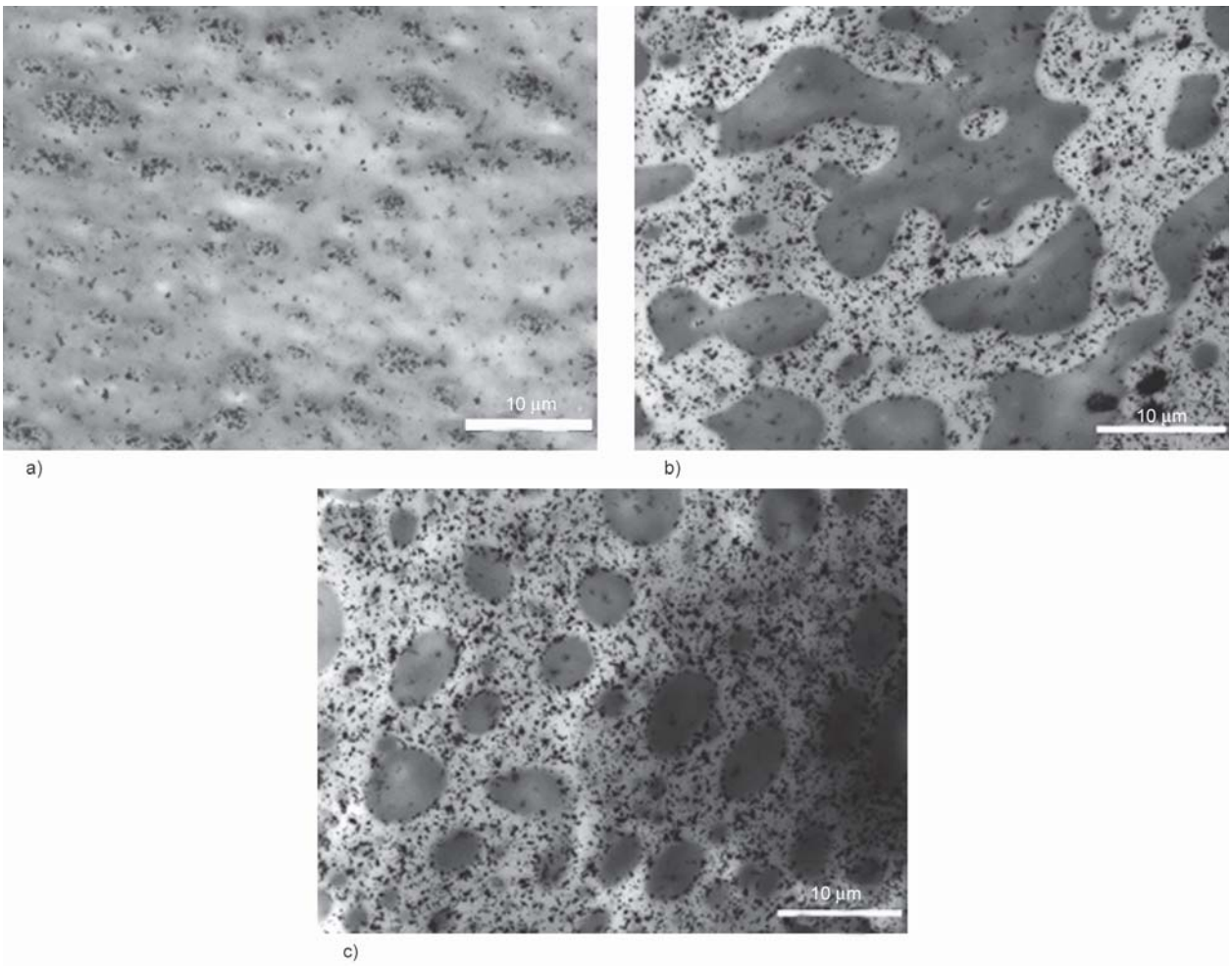

Figure 2. TEM micrographs of (a) 25/75, (b) 50/50, and (c) 75/25 w/w PLA/PHBV blends mixed with 3 phr TiO_2 nanoparticles.

continuous phase that contains much fewer nanoparticles, but there are also smaller spheres/ellipsoids with almost no nanoparticles within the larger nanoparticle-containing spheres/ellipsoids. This micrograph also shows more clearly the merging of the PLA spheres to start forming the continuous phase.

(3) Figure 1f clearly shows the newly formed PLA continuous phase with the PHBV spheres embedded in it, and again it is clear that the nanoparticles have a higher preference for the PLA than for the PHBV. Another observation from this micrograph is that there are clear cavities around the PHBV spheres. One gets the impression from these results that, when PLA is the minority phase, the interaction between the two phases is stronger than when PHBV is the minority phase. So far we do not have a clear explanation for this observation.

The TEM micrographs in Figure 2 to a large extent supports the observations in the SEM micrographs in Figure 1d–1f). In these micrographs the nanoparticles are visible as black spots that are fairly well dispersed, although small agglomerates are also visible.

3.2. Broadband dielectric spectroscopy of blends and nanocomposites

Broadband dielectric spectroscopy (BDS) is one of the most convenient, widely used, and versatile techniques to evaluate the dynamics of polymeric materials at wide ranges of time and length scales. In this study, we used this powerful tool to assess the affinity of TiO_2 nanoparticles for the PLA and PHBV phases. The data is interpreted in terms of the temperature behavior of the imaginary part of the dielectric permittivity (ε″) and the electric modulus (M''). Complex electric modulus (M^*) representation is widely used to analyze ionic conductivity in polymers. A pure conduction process is evidenced by a relaxation peak in the M'' vs. frequency (f) spectra with no peak observed in the corresponding ε″ vs. f spectra. When relaxation processes correspond to dipolar polymer chain motions, a relaxation peak appears in both the M'' and ε″ vs. f spectra. Long-range conductivity would result from electrode polarization, space charge, unintended ionic impurities in the sample, and it is evidenced by a large progressive increase of the ε″ and ε′ values at low f and higher temperatures. The complex electric modulus (M^*) is defined in Equation (1)–(3) [25–27]:

$$M^*(\omega) = \frac{1}{\varepsilon^*} = M' + M'' \tag{1}$$

$$M' = \frac{\varepsilon'}{\varepsilon'^2 + \varepsilon''^2} \tag{2}$$

$$M'' = \frac{\varepsilon''}{\varepsilon'^2 + \varepsilon''^2} \tag{3}$$

where M' and M'', ε′ and ε″ are the real and imaginary parts of the complex electric modulus and dielectric permittivity, respectively.

Figure 3 shows the ε″ and M'' vs. f spectra over a temperature range of –100 to 150 °C, for the neat PLA and PHBV samples. In the control PLA sample, three relaxations are clearly observed, namely the PLA β-relaxation and α-relaxations, and the Maxwell-Wagner-Sillars (MWS) relaxation. The PLA β-relaxation has two peak maxima at around –75 and 15 °C and is attributed to the twisting motions of the main chain [28–30]. Badia *et al*. [31] linked this relaxation to the specific movements of the terminal polar groups such as carboxyl, hydroxyl and ester in the PLA branches. The PLA α-relaxation has a peak maximum at around 75 °C and is associated with the long-range cooperative chain motions as we pass through the glass transition temperature (T_g) region [28–32]. The MWS relaxation above T_g is linked to the conduction behavior due to motions of the charge carriers and their accumulation at the interface of the crystalline and glassy phases of the polymer [31, 32].

The neat PHBV sample exhibits three relaxations namely the PHBV β-relaxation and α-relaxations, and the MWS relaxation, as shown in Figure 1b. The PHBV β-relaxation is a weak and broad relaxation with a peak maximum at around –30 °C, and is attributed to the cooperative motions of the methyl and ester groups [30, 33] or torsional vibrations of the main chains in the neighborhood of its local equilibrium conformation [34]. The PHBV α-relaxation accounts for the chain segmental mobility associated with the glass transition temperature and it is a very broad motion which splits into two peaks with maxima at –30 and 20 °C. The broadness and split of this peak could reflect the heterogeneous environment in which the chains are moving as it mainly reflects the large conformational rearrangement of the main chain in the amorphous region of the polymer [33, 35]. The MWS interfacial polarization peak at $T > T_g$ is related to the charge carriers build-up at the amorphous/crystalline

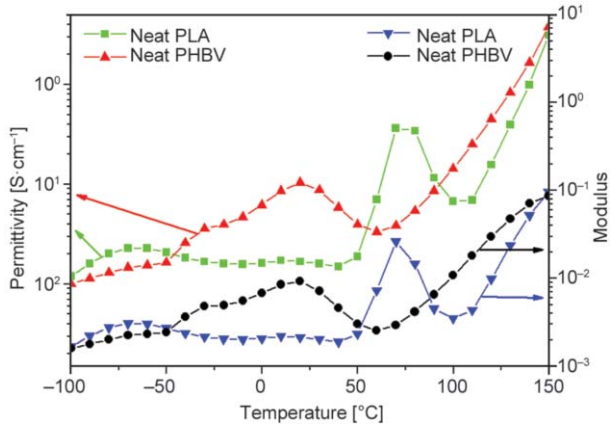

Figure 3. Temperature dependence of the imaginary part of the dielectric permittivity loss (ε″) and the electric modulus (*M*″) for control PLA and PHBV samples at a frequency of 1 kHz.

interface due to differences in conductivities of these phases [30, 33, 34].

Figure 4 shows the ε″ and *M*″ vs. *f* spectra, over a temperature range of –100 to 150 °C, for the 25/75, 50/50, and 75/25 w/w PLA/PHBV blends mixed with 3 phr TiO_2 nanoparticles. It is clear that the different relaxations associated with the T_g and sub-T_g motions remain unchanged, in terms of their peak positions, with the presence of TiO_2, except for the 75/25 PLA/PHBV blend containing 3 phr of the nanoparticles (Figure 4c). For this specific blend, the PLA α-relaxation peak broadens and shifts to a higher temperature, with a small shoulder around 75 °C, indicating a certain degree of interaction between the TiO_2 nanoparticles and the PLA polymer chains. These interactions slowed the long-range cooperative motions of the chains at the T_g and caused them to require much more activation energy to occur. This result supports the SEM and TEM observations, discussed above, that the nanoparticles have a higher preference for the PLA than for the PHBV phase. It is also clear that the PHBV T_g did not show a similar trend in the 25/75 PLA/PHBV blend, as shown in Figure 4a.

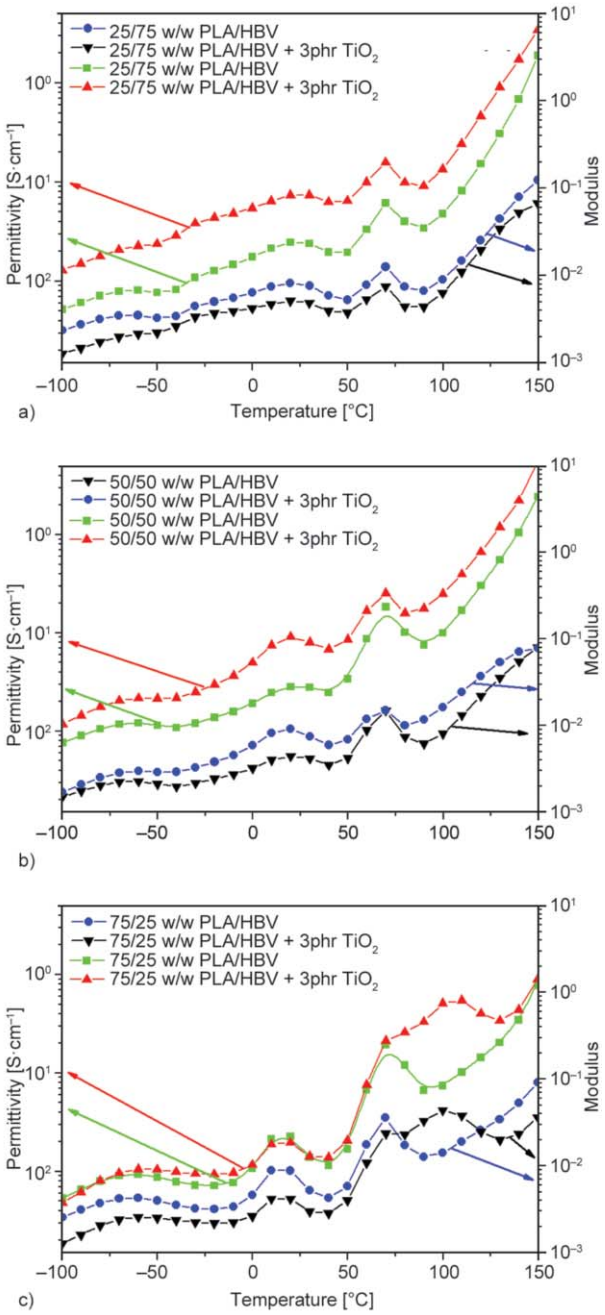

Figure 4. Temperature dependence of the imaginary part of the dielectric permittivity loss (ε″) and the electric modulus (*M*″) for the 25/75 (a), 50/50 (b), and 75/25 (c) w/w PLA/PHBV blends mixed with different percentages of TiO_2 nanoparticles, at a frequency of 1 kHz.

3.3. Thermal behavior of blends and nanocomposites

Figure 5a shows the cooling curves of the neat polymers and the 25/75, 50/50 and 75/25 w/w PLA/PHBV blends. Neat PHBV shows an intense, well defined crystallization peak at about 115 °C. The 25/75 w/w PLA/PHBV blend shows an equally well defined but less intense crystallization peak at almost exactly the same temperature. The smaller peak is obviously the result of the smaller PHBV fraction in this blend. It is, however, clear that the embedded PLA spheres in this blend composition had little influence on the PHBV crystallization behavior. For the 50/50 w/w PLA/PHBV blend the crystallization peak is broader and less well defined, and the crystallization occurs at a lower temperature. It seems as if the unusual morphology of the blend at this composition has an

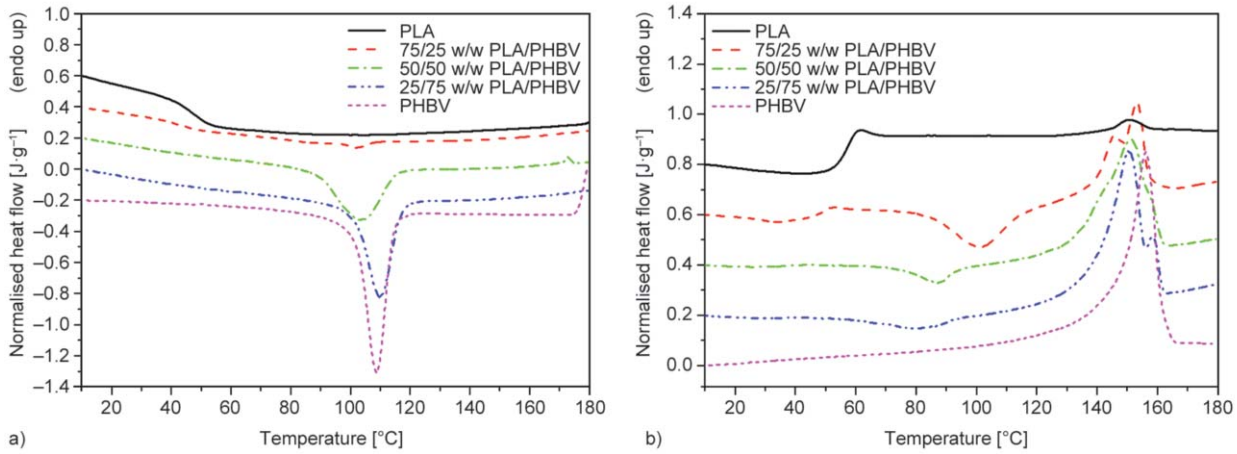

Figure 5. DSC (a) cooling and (b) second heating curves of neat PLA, neat PHBV and PLA/PHBV blends with different compositions.

influence on the crystallization behavior of the PHBV. It looks as if the formation of the crystalline PHBV spheres inside the PLA spheres is retarded by the presence of PLA. In this morphology, the PLA obviously also reduces the rate of PHBV crystallization, because the crystallization occurred over a broader temperature range. The inhibition of PHBV crystallization by PLA is especially clear when one looks at the DSC cooling curve of the 75/25 w/w PLA/PHBV sample. In this case there is a barely visible crystallization peak between 100 and 105 °C. The curve for neat PLA only shows its glass transition around 50–60 °C.

Inspection of the second heating curves of the different samples show that the PLA has a very intense glass transition around 60 °C, followed by a broad and weak cold crystallization exotherm in the region of 120–130 °C and a fairly well resolved melting peak at ~150 °C (Figure 5b). Analysis of the cold crystallization and melting peak areas show that the PLA did not possess any initial crystallinity. The PHBV only shows a well resolved melting peak around 150–160 °C, which makes it very difficult to distinguish between PLA and PHBV melting in the blends. All three blends show double melting peaks between 140 and 160 °C, which is probably an overlap of the melting peaks of respectively PLA and PHBV.

An interesting observation is, however, the influence of PLA:PHBV ratio on the cold crystallization temperature of PLA. In the presence of PHBV the PLA in the 75/25 w/w PLA/PHBV shows a much more resolved cold crystallization peak at a significantly lower temperature (~105 °C) than neat PLA (~125 °C). As the amount of PHBV in the sample increases from 25 to 75 w/w, the temperature of the PLA cold crystallization peak decreases from ~105 to ~80 °C. It is clear that the PHBV crystallites act as nucleation sites for PLA cold crystallization, and that higher PHBV contents, which would increase the contact area between PLA and PHBV, cause the cold crystallization process of PLA to start at lower temperatures.

The presence of TiO_2 nanoparticles, however, significantly changes the crystallization behavior of PHBV, and the cold crystallization behavior of PLA. Since some TiO_2 nanoparticles are present in the PHBV phase (Figures 1 and 2), the nanoparticles seem to nucleate the crystallization of PHBV, although they had little influence on the temperature at which the crystallization took place (compare Figures 5a and 6a). The neat PHBV + 3 phr TiO_2 shows a crystallization peak that is almost exactly the same as that of neat PHBV, while all three the blends show well resolved peaks with almost equal sharpness and at almost exactly the same temperature. The peak sizes are, however, not proportional to the respective amounts of PHBV in the different blend samples. Although it is clear that the TiO_2 does play a role in enhancing the nucleation and crystallization of PHBV in the different blends, the PLA still has an inhibiting effect on the growth of the PHBV crystals.

Figure 6b shows that the nanoparticles, that are mostly concentrated in the PLA phase of the blends, have an observable influence on the PLA cold crystallization. The effect is quite dramatic for neat PLA. In this case the DSC second heating curve shows a well-resolved and intense cold crystallization peak at 110 °C, followed by a double melting peak which indicates a melting-recrystallization-melting phenomenon. This observation is quite different from that observed in

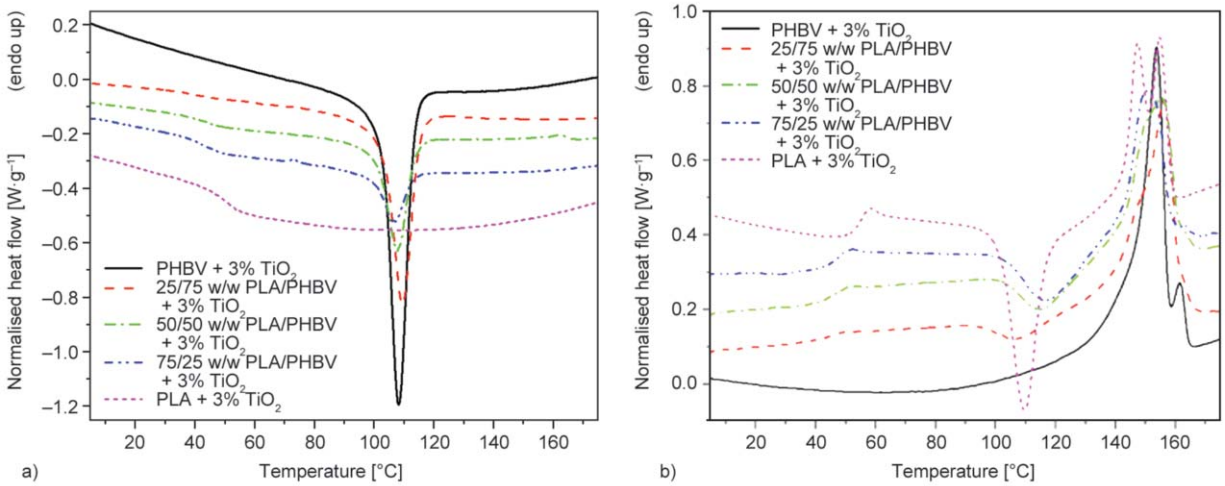

Figure 6. DSC (a) cooling and (b) second heating curves of neat PLA, neat PHBV and PLA/PHBV blends with different compositions, all containing 3 phr TiO_2 nanoparticles.

Figure 5b, which indicates that the TiO_2 nanoparticles have a strong nucleation and crystal growth effect on the PLA chains after PLA had gone through its glass transition. This effect is, however, quite subdued when PHBV is present. Although the crystallization peaks are slightly bigger and better defined compared to the blends without TiO_2 nanoparticles, the peak sizes do not correlate well with the blend ratios. It is further interesting that the cold crystallization of PLA in the nanocomposites occurs at significantly higher temperatures than those in the comparable blends. For some, at this stage unknown, reason the nucleation effect of the nanoparticles on PLA cold crystallization is not as effective as one would expect, and the nanoparticles seem to delay the onset of PLA cold crystallization. This can probably be explained through the uncommon but interesting morphologies of these blends, but further investigations with more sophisticated equipment may be needed to find an explanation for this phenomenon.

The isothermal crystallization kinetics analysis results, calculated according to the Avrami equation and by using the Origin software plugin developed by Lorenzo *et al*. [24], presented us with very interesting results. Since the PLA grade that we used did not crystallize on cooling, we expected to see only one isothermal crystallization peak at the investigated crystallization temperatures used for the different blends and nanocomposites. We found this to be the case for the 25/75 w/w PLA/PHBV blends without and with 3 phr TiO_2. However, as soon as a co-continuous phase started developing, and especially when PLA started becoming the major, continuous phase in the blends and nanocomposites, the isothermal crystallization curves showed two crystallization peaks (Figure 7). This was true for both the blends without and with nano-TiO_2, although no link can be drawn between the presence of nano-TiO_2 and the positions and/or sizes of the two crystallization peaks in these two blends.

The most probable explanation for this observation would be that PLA solidifies without crystallizing when it is the minor phase and forms spheres within the continuous PHBV phase, but when it becomes a sizable component in the blend, the isothermal crystallization of the PHBV also initiates the crystallization of the PLA, which is the second crystallization peak that we observed for these blends.

In order to confirm our explanation of this observation, we heated the 75/25 w/w PLA/PHBV blend to a temperature where all the thermal history was removed, cooled it to 0 °C, and re-heated it to a temperature above its melting point. This second heating curve in Figure 8 clearly shows the glass transition around 50 °C, followed by the cold crystallization around 100 °C, and the melting of both PLA and PHBV around 150 °C. However, when the sample was first kept isothermally at 119 °C for 40 min. before cooling to 0 °C and re-heating, the glass transition became very weak and the cold crystallization peak disappeared, and a much more intense and well-defined melting peak appeared around 140 °C. This confirms our conclusion that the isothermal crystallization of PHBV, when there were equally sized fractions of PLA and PHBV, or where the PLA fraction was bigger, initiated the isothermal crystallization of PLA, which was then clearly seen as a second crystallization peak in Figure 7.

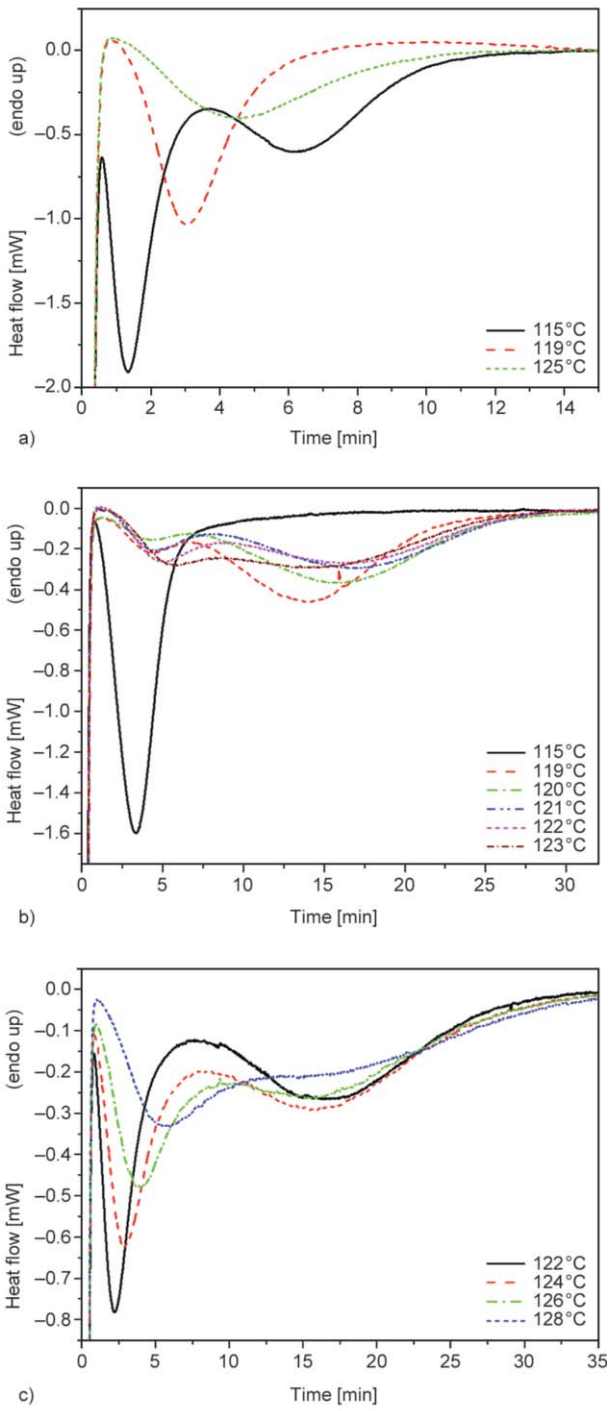

Figure 7. Isothermal crystallization curves of (a) 50/50 w/w PLA/PHBV, (b) 75/25 w/w PLA/PHBV, and (c) 75/25 w/w PLA/PHBV + 3 phr TiO_2.

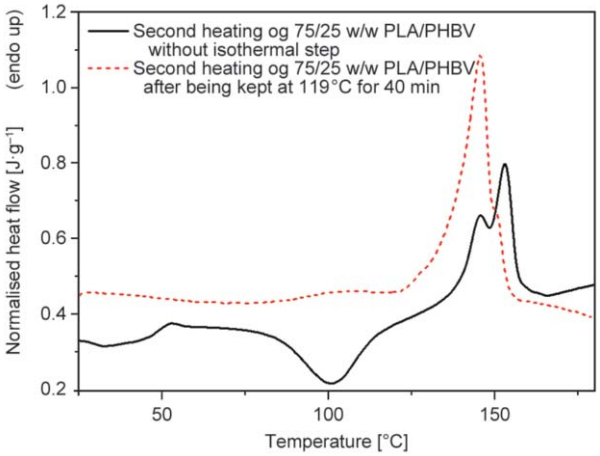

Figure 8. DSC second heating curves of 75/25 w/w PLA/PHBV without and with isothermal crystallization steps forming part of the thermal programme.

The isothermal crystallization of PLA, described above, unfortunately gave rise to very complex and atypical results when the inverse of the crystallization half-time was plotted as a function of the crystallization temperature (Figure 9). The reason is that in some cases there was only one crystallization peak (presumably that of PHBV), and in other cases there were two crystallization peaks (presumably those of PHBV and PLA). In the latter case the two peaks generally overlapped and it was not possible to do separate Avrami analyses on these peaks. The Avrami software plugin [24] was therefore applied to the overlapped combination of the two peaks, which gave rise to some adverse results (not shown).

However, when the results were separated as shown in Figure 9, one can clearly see the influence of the presence of nano-TiO_2 on the rates of crystallization of the different blends. In two of the blends (the 50/50 and 75/25 w/w PLA/PHBV blends) the rate of crystallization is clearly higher when 3 phr nano-TiO_2 was present, and this difference in crystallization rate became larger as the fraction of PLA in the blend increased. However, the 25/75 w/w PLA/PHBV blend (Figure 9a) showed little difference between the crystallization rates of the blends without and with nano-TiO_2 at crystallization temperatures between 115 and 130 °C. This can be explained by the fact that the TiO_2 was mostly present in the PLA phase, although small amounts could also be seen in the PHBV phase (as discussed in Section 3.1). This further confirms that PLA also crystallized during the isothermal crystallization process in the blends containing 50 wt% and more PLA.

Table 1 shows that the Avrami exponent values for most of the blends and nanocomposites fall between 2 and 3, which is an indication of instantaneous, heterogeneous nucleation and a mixture of two- and three-dimensional growth into axialites and spherulites. However, the 75/25 w/w PLA/PHBV samples (without and with TiO_2) generally showed values between 1.5 and 2.5, which further confirms the suppression of the growth of the PHBV crystals when

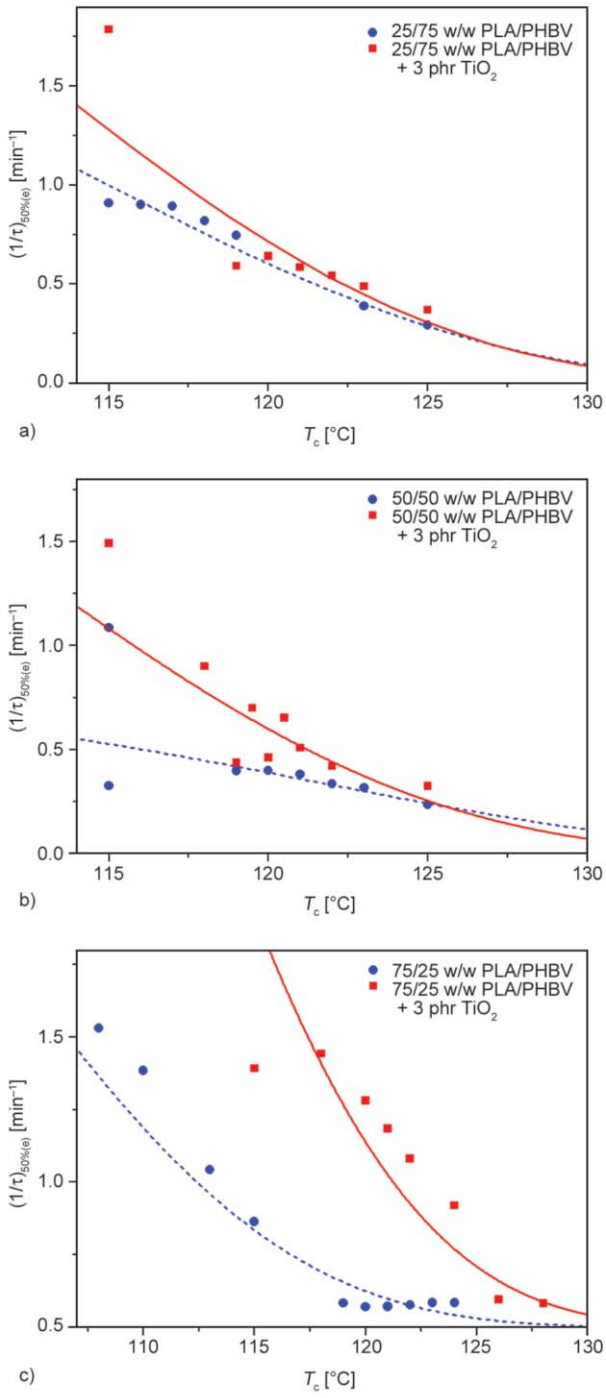

Figure 9. Comparison of the crystallization half-time as a function of isothermal crystallization temperature between the blends with and without 3 phr TiO_2. The symbols are the experimental values and the lines are fits to the Lauritzen and Hoffman theory.

PLA was the major phase. The blend morphology in each case obviously determined the nucleation and growth mechanism of the different components in the blends and nanocomposites, but it is almost impossible to directly relate the values observed in Figure 9 with the known morphology for each of the blends and nanocomposites.

3.4. Tensile properties

Table 2 summarizes the tensile properties of the different blends without and with 3 phr TiO_2. It is clear that PLA provides tensile strength and stiffness to the blends and nanocomposites, because the stress at break and Young's modulus values observably increased with increasing PLA content in the blends and nanocomposites. The influence of the presence and amount of TiO_2 nanoparticles on this property depended on the blend composition, which determined the blend morphology. Although there are some variations in the results, a general increase in tensile strength is observed with increasing TiO_2 content in the samples. TiO_2 clearly had a reinforcing effect on the investigated blends.

As in the case of the stress at break, a general increase was observed for the strain at break with increasing PLA and TiO_2 contents. However, because the values are so small, and because there are observable variations in the values, one cannot give too much significance to these values. Young's modulus for the 25 wt% PLA containing samples are observably lower than those of the 50 and 75 wt% PLA containing samples. One would expect Young's modulus to increase with increasing PLA content because of the much stiffer nature of this polymer, but it is interesting that the 50/50 and 75/25 w/w samples show almost the same Young's modulus within experimental error. This is probably because of the unusual morphology observed for the 50/50 w/w sample, which causes the PLA to have a larger than expected influence on the sample stiffness.

4. Conclusions

The morphology, crystallization behavior and mechanical properties of PLA, PHBV and their blends and nanocomposites with TiO_2 as filler were investigated using SEM, TEM, broadband dielectric spectroscopy, DSC and tensile testing. An uncommon morphology change was observed with increasing PLA content in the blends, and this caused deviations from the typical crystallization rate vs. crystallization temperature curves. It was also observed that PLA, which do not normally crystallize during the cooling of the sample, showed isothermal crystallization for certain blend compositions. TiO_2 was found to be mainly present in the PLA phase, although small amounts of TiO_2 nanoparticles were also observed in the PHBV phase. This observation was confirmed through broadband dielectric analysis.

Table 1. Avrami parameter as function of crystallization temperature for the different investigated blends and composites.

	Avrami index, *n*							
T_c [°C]	Neat PHBV	PHBV + 3 phr TiO_2	25/75 w/w PLA/PHBV	50/50 w/w PLA/PHBV	75/25 w/w PLA/PHBV	25/75 w/w PLA/PHBV + 3 phr TiO_2	50/50 w/w PLA/PHBV + 3 phr TiO_2	75/25 w/w PLA/PHBV + 3 phr TiO_2
108	–	–	–	–	2.3	–	–	–
110	–	–	–	–	2.3	–	–	–
113	–	–	–	–	2.8	–	–	–
115	2.7	2.9	2.8	–	2.7	2.6	2.3	1.9
116	–	2.8	2.8	–	–	–	–	–
117	2.7	2.8	2.6	–	–	–	–	–
118	2.8	2.7	2.6	–	–	–	2.3	2.1
119	3.1	2.7	2.5	3.0	1.5	3.0	2.9	–
119.5	–	–	–	–	–	–	2.3	–
120	3.1	2.8	–	2.7	1.4	2.5	2.7	2.3
120.5	–	–	–	–	–	–	2.5	–
121	3.0	2.8	–	2.7	1.7	2.6	2.4	2.5
122	3.0	–	–	2.6	2.2	2.5	2.6	2.1
123	3.0	2.7	2.6	2.6	2.3	2.5	–	–
124	3.0	–	–	–	2.6	–	–	2.1
125	–	2.8	2.6	2.6	–	2.5	2.4	–
126	–	–	–	–	–	–	–	2.1
128	–	–	–	–	–	–	–	2.2
130	–	–	–	–	–	–	–	2.2

Table 2. Tensile properties of the investigated blend and nanocomposite samples.

PLA/PHBV/TiO_2	σ [MPa]	ε [%]	*E* [MPa]
25/75/0	9.7±2.6	1.6±0.8	1141±54
25/75/1	11.9±2.5	1.9±0.5	1183±98
25/75/3	12.7±2.4	2.0±0.5	1201±137
50/50/0	17.9±2.7	2.4±0.6	1521±99
50/50/1	20.4±1.2	2.9±0.5	1405±91
50/50/3	18.1±2.7	2.4±0.4	1351±106
75/25/0	23.9±4.5	2.5±0.3	1621±140
75/25/1	21.5±6.9	2.4±0.7	1446±112
75/25/3	27.7±4.3	3.1±0.4	1520±68

σ = stress at break; ε = strain at break; *E* = Young's modulus

The blend composition, as well as the presence of TiO_2 nanoparticles, had an influence on the cold crystallization of the PLA. The tensile properties changed with blend and nanocomposite composition, and these changes could to a certain extent be related to the respective morphologies.

References

[1] AlMaadeed M., Özerkan G., Kahraman R., Madi N.: Recycling plastic in Qatar – Current situation and future prospects. Materials Technology Unit, Qatar University (2010).

[2] Nomai J., Suksut B., Schlarb A. K.: Crystallization behavior of poly(lactic acid)/titanium dioxide nanocomposites. KMUTNB International Journal of Applied Science and Technology, **8**, 251–258 (2015). https://doi.org/10.14416/j.ijast.2015.10.003

[3] Day M., Nawaby A. V., Liao X.: A DSC study of the crystallization behaviour of polylactic acid and its nanocomposites. Journal of Thermal Analysis and Calorimetry, **86**, 623–629 (2006). https://doi.org/10.1007/s10973-006-7717-9

[4] Battegazzore D., Bocchini S., Frache A.: Crystallization kinetics of poly(lactic acid)-talc composites. Express Polymer Letters, **5**, 849–858 (2011). https://doi.org/10.3144/expresspolymlett.2011.84

[5] Yu H-Y., Qin Z-Y., Zhou Z.: Cellulose nanocrystals as green fillers to improve crystallization and hydrophilic property of poly(3-hydroxybutyrate-*co*-3-hydroxyvalerate). Progress in Natural Science: Materials International, **21**, 478–484 (2011). https://doi.org/10.1016/S1002-0071(12)60086-0

[6] Hosoda N., Lee E-H., Tsujimoto T., Uyama H.: Phase separation-induced crystallization of poly(3-hydroxybutyrate-*co*-hydroxyvalerate) by branched poly(lactic acid). Industrial and Engineering Chemistry Research, **52**, 1548–1553 (2013). https://doi.org/10.1021/ie3011275

[7] Li H., Lu X., Yang H., Hu J.: Non-isothermal crystallization of P($_3$HB-*co*-$_4$HB)/PLA blends. Journal of Thermal Analysis and Calorimetry, **122**, 817–829 (2015). https://doi.org/10.1007/s10973-015-4824-5

[8] Zhao H., Cui Z., Wang X., Turng L-S., Peng X.: Processing and characterization of solid and microcellular poly(lactic acid)/polyhydroxybutyrate-valerate (PLA/PHBV) blends and PLA/PHBV/clay nanocomposites. Composites Part B: Engineering, **51**, 79–91 (2013). https://doi.org/10.1016/j.compositesb.2013.02.034

[9] Zembouai I., Bruzaud S., Kaci M., Benhamida A., Corre Y-M., Grohens Y., Lopez-Cuesta J-M.: Synergistic effect of compatibilizer and cloisite 30B on the functional properties of poly(3-hydroxybutyrate-*co*-3-hydroxyvalerate)/polylactide blends. Polymer Engineering and Science, **54**, 2239–2251 (2013). https://doi.org/10.1002/pen.23776

[10] John M. J.: Biopolymer blends based on polylactic acid and polyhydroxy butyrate-*co*-valerate: Effect of clay on mechanical and thermal properties. Polymer Composites, **36**, 2042–2050 (2015). https://doi.org/10.1002/pc.23114

[11] Zembouai I., Bruzaud S., Kaci M., Benhamida A., Corre A. M., Grohens Y., Taguet A., Lopez-Cuesta J-M.: Poly (3-hydroxybutyrate-*co*-3-hydroxyvalerate)/polylactide blends: Thermal stability, flammability and thermo-mechanical behavior. Journal of Polymers and the Environment, **22**, 131–139 (2014). https://doi.org/10.1007/s10924-013-0626-7

[12] Zembouai I., Kaci M., Bruzaud S., Benhamida A., Corre Y-M., Grohens Y.: A study of morphological, thermal, rheological and barrier properties of poly(3-hydroxybutyrate-*co*-3-hydroxyvalerate)/polylactide blends prepared by melt mixing. Polymer Testing, **32**, 842–851 (2013). https://doi.org/10.1016/j.polymertesting.2013.04.004

[13] Bledzki A. K., Jaszkiewicz A.: Mechanical performance of biocomposites based on PLA and PHBV reinforced with natural fibres – A comparative study to PP. Composites Science and Technology, **70**, 1687–1696 (2010). https://doi.org/10.1016/j.compscitech.2010.06.005

[14] Modi S., Koelling K., Vodovotz Y.: Assessing the mechanical, phase inversion, and rheological properties of poly-[(R)-3-hydroxybutyrate-*co*-(R)-3-hydroxyvalerate] (PHBV) blended with poly-(L-lactic acid) (PLA). European Polymer Journal, **49**, 3681–3690 (2013). https://doi.org/10.1016/j.eurpolymj.2013.07.036

[15] Nanda M. R., Misra M. I., Mohanty A. K.: The effects of process engineering on the performance of PLA and PHBV blends. Macromolecular Materials and Engineering, **296**, 719–728 (2011). https://doi.org/10.1002/mame.201000417

[16] Mofokeng J. P., Luyt A. S.: Dynamic mechanical properties of PLA/PHBV, PLA/PCL, PHBV/PCL blends and their nanocomposites with TiO_2 as nanofiller. Thermochimica Acta, **613**, 41–53 (2015). https://doi.org/10.1016/j.tca.2015.05.019

[17] Ma P., Spoelstra A. B., Schmit P., Lemstra P. J.: Toughening of poly (lactic acid) by poly (β-hydroxybutyrate-*co*-β-hydroxyvalerate) with high β-hydroxyvalerate content. European Polymer Journal, **49**, 1523–1531 (2013). https://doi.org/10.1016/j.eurpolymj.2013.01.016

[18] Ferreira B. M. P., Zavaglia C. A. C., Duek E. A. R.: Films of PLLA/PHBV: Thermal, morphological, and mechanical characterization. Journal of Applied Polymer Science, **86**, 2898–2906 (2002). https://doi.org/10.1002/app.11334

[19] Wagner A., Poursorkhabi V., Mohanty A. K., Misra M.: Analysis of porous electrospun fibers from poly(L-lactic acid)/poly(3-hydroxybutyrate-*co*-3-hydroxyvalerate) blends. ACS Sustainable Chemistry and Engineering, **2**, 1976–1982 (2014). https://doi.org/10.1021/sc5000495

[20] Richards E., Rizvi R., Chow A., Naguib H.: Biodegradable composite foams of PLA and PHBV using subcritical CO_2. Journal of Polymers and the Environment, **16**, 258–266 (2008). https://doi.org/10.1007/s10924-008-0110-y

[21] Buzarovska A., Grozdanov A., Avella M., Gentile G., Errico M.: Poly(hydroxybutyrate-*co*-hydroxyvalerate)/titanium dioxide nanocomposites: A degradation study. Journal of Applied Polymer Science, **114**, 3118–3124 (2009). https://doi.org/10.1002/app.30867

[22] Luo Y-B., Wang X-L., Wang Y-Z.: Effect of TiO_2 nanoparticles on the long-term hydrolytic degradation behavior of PLA. Polymer Degradation and Stability, **97**, 721–728 (2012). https://doi.org/10.1016/j.polymdegradstab.2012.02.011

[23] Mofokeng J. P., Luyt A. S.: Morphology and thermal degradation studies of melt-mixed PLA/PHBV biodegradable polymer blend nanocomposites with TiO_2 as filler. Journal of Applied Polymer Science, **132**, 42138/1–42138/11 (2015). https://doi.org/10.1002/app.42138

[24] Lorenzo A. T., Arnal M. L., Albuerne J., Müller A. J.: DSC isothermal polymer crystallization kinetics measurements and the use of the Avrami equation to fit the data: Guidelines to avoid common problems. Polymer Testing, **26**, 222–231 (2007). https://doi.org/10.1016/j.polymertesting.2006.10.005

[25] McCrum N. G., Read B. E., Williams G.: Anelastic and dielectric effects in polymeric solids. Wiley, London (1967).

[26] Macedo P. B., Moynihan C. T., Bose R.: The role of ionic diffusion in polarization in vitreous ionic conductors. Physics and Chemistry Glasses, **13**, 171–179 (1972).

[27] Howell F. S., Bose R. A., Macedo P. B., Moynihan C. T.: Electrical relaxation in a glass-forming molten salt. Journal of Physical Chemistry, **78**, 639–648 (1975). https://doi.org/10.1021/j100599a016

[28] Delpouve N., Delbreilh L., Stoclet G., Saiter A., Dargent E.: Structural dependence of the molecular mobility in the amorphous fractions of polylactide. Macromolecules, **47**, 5186–5197 (2014). https://doi.org/10.1021/ma500839p

[29] Brás A. R., Malik P., Dionísio M., Mano J. F.: Influence of crystallinity in molecular motions of poly(L-lactic acid) investigated by dielectric relaxation spectroscopy. Macromolecules, **41**, 6419–6430 (2008). https://doi.org/10.1021/ma800842a

[30] Hegde V. J.: Dielectric study of biodegradable and/or bio-based polymeric materials. PhD Thesis, Université Grenoble Alpes, Grenoble (2017).

[31] Badia J. D., Monreal L., de Juano-Arbona V. S., Ribes-Greus A.: Dielectric spectroscopy of recycled polylactide. Polymer Degradation and Stability, **107**, 21–27 (2014). https://doi.org/10.1016/j.polymdegradstab.2014.04.023

[32] Dichtl C., Sippel P., Krohns S.: Dielectric properties of 3D printed polylactic acid. Advances in Materials Science and Engineering, **2017**, 6913835/1–6913835/10 (2017). https://doi.org/10.1155/2017/6913835

[33] Fahmy T., Abdelwahed H. G., Ahmed M. T., El-kotp A., Abdelwahed H. G., Alshaeer M. Y.: Broadband dielectric spectroscopy and electric modulus analysis of poly(3-hydroxybutyrate-*co*-3-hydroxyvalerate) and related copolymers films. International Journal of Physics and Applications, **8**, 1–14 (2016).

[34] Ohki Y., Fuse N., Hikosaka S., Takemura Y., Mizuno M., Fukunaga K.: Complex permittivity spectra of several insulating polymers at electrical and THz frequencies. in 'IEEE Conference on Electrical Insulation and Dielectric Phenomena, Virginia Beach, Virginia' 7–10 (2009).

[35] Yang Y., Ke S., Ren L., Wang Y., Li Y., Huang H.: Dielectric spectroscopy of biodegradable poly(3-hydroxybutyrate-*co*-3-hydroxyhexanoate) films. European Polymer Journal, **48**, 79–85 (2012). https://doi.org/10.1016/j.eurpolymj.2011.10.002